Leveraging Metal Complexes for Microsecond Lifetime-Based Chloride Sensing

Jared Morse[#1], Nnamdi Ofodum[#1], Fung-Kit Tang[#1], Matthias Schmidt[1], Xiaocun Lu[1*], Kaho Leung[1*]

[1]*Department of Chemistry & Biomolecular Science, Clarkson University, NY, 13676, United States*

**Correspondence to: xlu@clarkson.edu (X.L.), kleung@clarkson.edu (K.L.)*

[#]*These authors contributed equally.*

Abstract:

Chloride is the most abundant anion in cell physiology and plays many critical roles in maintaining cellular homeostasis. However, current chloride sensors are rare, with inherent sensitivity in their emission properties, such as vulnerability to pH changes or short emission lifetimes. These limitations restrict their application in aqueous media and imaging. In this work, we employed a transition metal complex bearing pyridinium as a recognition unit for chloride and studied the phosphorescence emission properties. Iridium(III) complex **1** was synthesized as an alternative chloride-sensitive luminophore. The conjugable design also allows customization for desired applications. Complex **1** exhibited high sensitivity and selectivity in chloride sensing across different physiological environments, regardless of pH fluctuation and ionic strength. Additionally, complex **1** featured a long microsecond emission lifetime. The chloride sensing ability of complex **1** can be measured through both luminescence intensity and long-lived phosphorescent lifetime simultaneously, providing an alternative potential route for chloride imaging.

Graphical abstract:

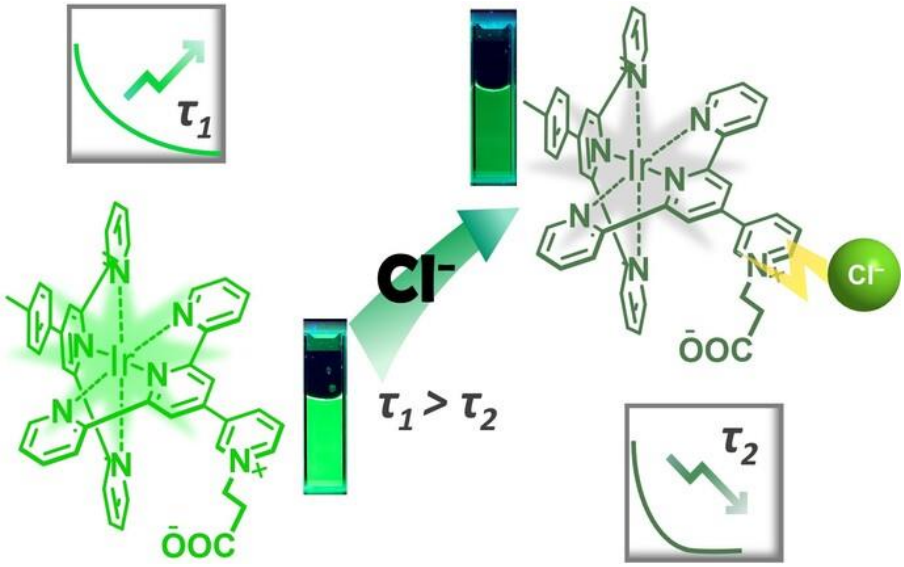

Keywords:

Chloride, chloride detection, chloride-sensitive luminophore, iridium complex

Introduction

Chloride is the most abundant intracellular ion beside sodium, it mediates a multitude of different processes such as cell volume,[1,2] membrane potential, and lysosome homeostasis.[3–6] The concentration of chloride exhibits significant variability across organelles.[7] Overall cellular homeostasis relies on chloride balance and hence chloride levels are important parameters to assess various pathology. Dysregulation of physiological chloride has been observed in various diseases, for example, lysosomal storage disorders,[8–11] cystic fibrosis,[12] and osteoporosis.[13] Therefore, live cell chloride imaging is an important tool to investigate chloride homeostasis.

Fluorescent protein such as commercially available Premo™ halide sensor is often used to image intracellular chloride. However, the major disadvantage associated with protein-based chloride sensors lies in their vulnerability to pH variations. The sensitivity of Cl^- decreases as the pH lowers in acidic environments.[14] Organic fluorophores that carry quinolinium and acridinium groups could be quenched by halide ions. For examples, *N*-(ethoxycarbonylmethyl)-6-methoxyquinolinium bromide (MQAE), 6-methoxy-*N*-(3-sulfopropyl)quinolinium (SPQ) and 10,10′-bis[3-carboxypropyl]-9,9′-biacridinium dinitrate (BAC) fluorophores have been used as chloride sensors as well as chloride transport assays.[15–20] However, long emission lifetime chloride indicator are rare in literature. On the other hand, time-resolved fluorescence detection has attracted more attention recently as an imaging technique to acquire more information beyond luminescence intensities. Photoluminescence lifetimes are intrinsic physical properties of a sensor,[21,22] the lifetime signal is strongly influenced by the analytes in the surrounding environment but remains unaffected by the sensor concentration. Therefore, lifetime-based chloride detection can overcome challenges associated with uneven probe uptake and enable quantitative measurement. Additionally, time-resolved imaging of long-lifetime fluorophores can also eliminate background autofluorescence in biological samples. Nevertheless, existing chloride indicators fall in the nanosecond scale, which is short for the effective use in time-resolved fluorescence imaging or in samples with high autofluorescence. Therefore, sensors with long emission lifetimes would be exceptional candidates for time-resolved fluorescence and can be used to distinguish from autofluorescence that carry short emission lifetimes, hence achieving quantitative measurement with greater sensitivity.

Cyclometalated iridium(III) complexes have been extensively explored for their versatile applications such as light emitting diodes,[23,24] photocatalysts,[24] phototherapeutic agents and cell imaging dyes.[25,26] Compared to organic fluorophores with nanosecond lifetime, iridium(III) complexes display microsecond emissive lifetime, and the lifetime differences fall in an order of magnitude for potential use in time-resolved measurement. By temporally aligning the time gate after the completion of the inherent autofluorescence delay, researchers can selectively capture the signal of iridium(III) complex, thereby acquiring an image devoid of autofluorescence interference. Another advantage of employing transition metal complexes as the molecular probe lies in its modular synthesis capabilities. Through the modification of coordinating ligands, we can systematically fine-tune the photo-physical properties of the complexes. This capability could significantly aid researchers in elucidating methods to enhance dye performance and establish structure-property relationships for further development.[26,27]

Given the inherent advantages exhibited by iridium(III) complexes as luminescent fluorophores, our aim is to formulate a long emission lifetimes, pH-independent, conjugable, chloride-sensitive fluorophore with sensitivity to changes in physiological chloride concentration. Here, we synthesized a conjugable, bis-tridentate iridium(III) complex **1** as a chloride sensitive fluorophore. Through the incorporation of a N^N^N-coordinating tridentate ligand featuring a pyridinium ion, complex **1** attains the capacity to selectively detect chloride at a physiological level. Complex **1** exhibits the chloride detecting ability in a pH-independent manner. Additionally, it exhibits selective detection of chloride over various biological anions at physiological levels. We then leverage complex **1** for lifetime-based chloride measurements. Complex **1**

serves as a proof-of-concept demonstrating that iridium(III) complexes can effectively function as chloride-sensitive lumiphores, thereby offering valuable insights into fluorescence lifetime imaging techniques for cellular chloride.

Results and discussion

Design, synthesis and characterization of chloride-sensitive iridium complex.

Quinolinium and acridinium are the major recognition motifs of chloride-sensitive fluorophores. To make an indicator with long emission lifetime for Cl^-, we seek to incorporate pyridinium group into Ir(III) complex for chloride-sensing, achieving chloride detection as a function of luminescent intensity simultaneously. It has been reported that chloride ions quench the luminescence of iridium(III) bis-terpyridine complexes incorporating pendent *N*-methylpyridinium groups.[28] However, the investigation is confined solely to the phenomenon of photoluminescence quenching. The analysis of chloride-sensitive fluorophores remained unexplored. Alternatively, in response to the growing demand for conjugatable functional fluorophores, we intend to synthesize a conjugatable iridium(III) bis-tridentate complex carrying a pyridinium group in a stepwise approach (Figure 1). In brief, terpyridine ligand **A** was prepared by Kröhnke pyridine synthesis using 3-pyridinecarboxaldehyde and 2-acetylpyridine, which reacted with complex **B** to afford complex **C**. Then the pendant pyridine moiety on **C** was alkylated using 3-iodopropionic acid to give the iridium(III) complex **1**. All the compounds have been fully characterized by NMR and HRMS (Figure S3−S12). Complex **1** features a pyridinium group intended to confer chloride-sensitivity. Through this modified synthetic approach, the linking ligand can be modulated for conjugation with different substrates or ligands, which provides an advantage for integrating with imaging carrier or sensing devices in the future. For a pilot investigation of complex **1** regarding potential use as an imaging agent, cell viability assay was also performed to evaluate the cytotoxicity of complex **1**. Complex **1** showed almost no cytotoxicity up to a high concentration at 25 μM (Figure S2). The absorption and fluorescence spectra of air-equilibrated aqueous solution of complex **1** are shown in Figure 2a-c. Complex **1** exhibited a board emission maximum of 510 nm in aqueous solution, and a board excitation peak from UV region to 370 nm (Figure 2a). A large stoke shift of 150 nm was observed when **1** was excited at 360 nm, this characteristic of phosphorescent Ir(III) complexes help minimize crosstalk from excitation sources and enhance sensitivity. There is no observable alteration in the absorption spectra of **1** upon the addition of 100 mM of Cl^- (Figure 2c), suggesting **1** remained structurally intact and was dynamically quenched by Cl^-. Moreover, the phosphorescence intensity of **1** experienced a naked-eye observable reduction in the presence of 100 mM of Cl^- (Figure 2b). Overall, the result matched our expectation that the emission of complex **1** decreased with increasing [Cl^-] via a collisional quenching effect.

Complex 1 exhibits luminescence variations in response to physiologically relevant chloride concentrations

Given the promising chloride-quenching behaviour exhibited by complex **1**, the concentration dependent luminescence response of complex **1** was investigated. Complex **1** was titrated with increasing Cl^- concentration. Under excitation at 360 nm, luminescence intensity at 510 nm dropped gradually with increased Cl^- concentration from 0 mM up to 150 mM (Figure 2d). The luminescence intensity of complex **1** exponentially decrease upon addition of increasing concentration of Cl^- (Figure 2e, red). Within the physiologically relevant chloride concentration range 10–120 mM, there is a linear relationship between I_o/I_F and [Cl^-], and this phenomenon followed the Stern–Volmer relationship. To confirm whether complex **1** could selectively detect Cl^-, the luminescence response of complex **1** towards various biologically relevant anions were examined (Figure 2f). No significant response of complex **1** was observed in the presence of 150 mM of various anions including phosphates, nitrates, sulphates and acetate. The sensor complex **1** showed a high selectivity towards Cl^- while it was insensitive to many biologically relevant cations and anions even at a much higher concentration found in physiology. Since complex **1** detects Cl^-

through a collisional quenching mechanism, other heavier halide ions such as Br^- or I^- may also exhibit a quenching effect. Hence, the effect of other halogen species was also investigated, both Br^- or I^- ions exert a greater extent of luminescence quenching of complex **1** at the same concentration of 100 mM (Figure S1). However, the abundance of Br^- and I^- in physiological cellular environments is significantly lower compared to Cl^-, therefore their impact on the luminescence of complex **1** in biological systems is minimal.[29,30]

Complex 1 selectively detects chloride in a pH independent manner

In sensor application pH is an important parameter to be considered. Cl^- exists in stable anionic form in aqueous medium due to a low pKa, –7 of HCl/Cl^- equilibrium. However, existing sensors having different inherent pKa values that may be susceptible to pH variation and lead to possible interference of detection. From the viewpoint of cellular biology, the physiological pH of body fluids as well as small subcellular organelle components alters with different cell conditions. For instance, the intracellular pH varies from organelle to organelle, ranging from pH 7.8 to pH 4.5 which may affect sensor operation, hence the detection of Cl^- in pH-independence manor is highly desired for analysis in biological environments. The effect of pH on complex **1** and the chloride sensing performance was further investigated. Minimal deviation was observed when comparing each pH by overlaying each Stern-Volmer plot (Figure 3b). Complex **1** displayed a similar chloride sensitvity from pH 4.5 to 7.2 in sodium phosphate buffer (20 mM). A consistent 3-fold change in I_o/I_F have been recorded across physiological pH range at 150 mM Cl^- (Figure 3c). Through integrating the two parameters (pH and [Cl^-]), a 3D calibration surface plot is obtained that shows the detection (I_o/I_F) is linear proportional to [Cl^-] and independent of pH (Figure 3a). Subsequently, we simply altered the pH in neutral and acidic pH environments (pH 7 and pH 4.5) and determined the lifetime decay in the absence or presence of 100 mM Cl^- (Figure 3d-f). Under air-equilibrated aqueous condition, complex **1** has a phosphorescence lifetime of 1.5 µs, while it decreased to 0.8 µs upon addition of 100 mM Cl^-. Neither neutral or acidic pH exerted an effect on the phosphorescent lifetime at respective Cl^- concentrations.

Eligibility of complex 1 as a chloride-sensitive dye in physiological environments.

In the physiological environment, a plethora of electrolyte species exist. This presence of ionic species may weaken the interaction with the negatively charged chloride and positively charged complex **1**, thereby exerting potential detection interference. To further investigate and therefore mimic the physiological ionic environments, we utilized buffer with physiological ion levels for *in vitro* calibration to rule out any off-target effects. Subsequently, we investigated the chloride detecting ability of complex **1** in various pH in a physiological buffered environment. Similarly, no significant change in I_o/I_F values across different pH values in physiological buffer was observed (Figure 4b). The interference from other ionic salts on the chloride sensing property was also investigated in a physiological environment. We employed a Stern-Volmer plot of ionic titrations at multiple pH in the presence of other ionic species, no significant I_o/I_F change was observed when complex **1** was titrated with KNO_3, KH_2PO_4, and K_2SO_4 across different indicated concentrations and pH values (Figure 4c). As a positive comparison, complex **1** only showed luminescence quenching in the presence of KCl (Figure 4c). The 3D surface calibration plot was consistent and reproduced a similar sensing trend (linearity of I_o/I_F against [Cl^-]) in the presence of various ionic salts (Figure 4a).The phosphorescence lifetime of complex **1** in the same physiologically mimicked environment was investigated (Figure 4d-e).The phosphorescence lifetime decreased steadily from 1.5 µs at 0 mM [Cl^-] to 0.8 µs at 100 mM [Cl^-]. The lifetime decay values with or without Cl^- were consistent across the entire study. Hence, it indicates that the lifetime of complex **1** is a unique intrinsic property that only changes upon chloride environments. This intrinsic lifetime property solely correlates with different concentrations of chloride, while remaining unaffected in the presence of other ionic salts and pH alteration. It is worth noting that this lifetime property shows promise with prospective uses in FLIM. Overall, all the data

indicated the chloride selectivity and pH insensitivity properties, therefore complex **1** could serve as a reliable chloride indicator in the complex cellular environments and pH range.

Conclusion

The development of phosphorescent indicators with long emission lifetime is crucial for applications in time-resolved imaging. Currently, in literature the report of these indicators is sparse. It is necessary to investigate more opportunity in the Cl^- imaging field. As a proof of concept, highly phosphorescent Ir(III) complex **1** has been synthesized and characterized. This new approach provides flexibility for substrate conjugation to functionalize different materials for sensing or perhaps catalysis purposes. Our results demonstrated that complex **1** was capable of monitoring chloride dynamics in terms of intensity and lifetime simultaneously, while displaying no interference from other tested ionic salts. Most importantly, complex **1** is soluble in aqueous medium and its analytical characteristics was investigated with different pH and buffers, providing the optimization and testing conditions for Cl^-. Complex **1** features a large stoke shift of 150 nm with green emission at 510 nm, and robust chloride sensing ability in a pH independent fashion in physiological ranges, which is beneficial as a potential imaging agent. This preliminary study has demonstrated the use of a phosphorescent complex as a reliable Cl^- sensor, further developments and applications are undergoing to provide new options in studying chloride physiology are needed.

Methods

General synthetic materials

Chemicals or reagents were purchased from Fisher Chemicals, Sigma Aldrich, TCI, Thermo Fisher, Ambeed or Alfa Aesar and used as received. All solvents were used directly without further treatment or distillation. Silica gel 60 (70–230 mesh, Supelco®) was used for column chromatography. Thin Layer Chromatography (TLC) was performed using F_{254} silica (aluminum sheet back plates, Supelco®).

Materials for *in vitro* studies

Sodium phosphate monobasic, sodium phosphate dibasic, and sodium acetate was purchased from Fisher Scientific (Hampton, USA). Potassium nitrate, sodium nitrate, calcium nitrate, magnesium nitrate, sodium chloride, magnesium chloride, potassium sulphate, and magnesium sulphate were purchased from Sigma-Aldrich (St Louis, MA, USA).

in vitro fluorescence measurements

UV–Vis absorption spectra was collected on a Hewlett Packard HP 8453 spectrometer and fluorescence spectra were taken using SpectraMaxTM i3/i3x multi-mode plate reader or Varian Cary eclipse fluorescence spectrophotometer. Complex **1** was dissolved in dimethyl sulfoxide (DMSO) to create a 5 mM stock solution. This stock was subsequently diluted to achieve a final concentration of 10 µM, utilizing 20 mM sodium phosphate buffer supplemented with 150 mM KNO_3, 5 mM $NaNO_3$, 1 mM $Ca(NO_3)_2$ and $Mg(NO_3)_2$ across a range of pH values. The emission spectra of **1** was acquired by exciting the sample at 365 nm. To study the chloride sensitivity of **1**, final [Cl^-] ranging between 0 mM to 150 mM was achieved by adding microlitre aliquots of 4 M KCl to the samples. To study selectivity of **1**, final concentrations of 100 mM of various salts was achieved by adding microlitre aliquots of 0.5−4 M stocks. The analysis of *in vitro* measurements for **1** was conducted by assessing the fold change, as annotated by the ratio of initial intensity (I_0) to final intensity (I_F). This is from 0 mM to 150 mM of each indicated ions, where I_0 is the intensity at 0 mM and I_F at respected final concentration of analyte.

in vitro fluorescence lifetime measurements

Fluorescence lifetime data was collected using an Edinburgh FLS1000 spectrometer. Complex **1** was dissolved in dimethyl sulfoxide (DMSO) to prepare a 5 mM stock solution, which was then diluted to a final concentration of 100 µM in a 5 mM sodium phosphate buffer at pH 4.5 or 7. For the chloride sensitivity

analysis, chloride concentrations ranging from 0 mM to 100 mM was achieved by adding microliter aliquots of 4 M KCl to each sample. For samples in physiological buffered environments, 5 mM sodium phosphate buffer supplemented with 150 mM KNO_3, 5 mM $NaNO_3$, 1 mM $Ca(NO_3)_2$ and 1mM $Mg(NO_3)_2$ was used. Samples were excited with a pulsed LED (280 nm) every 10 µs, and the decay was monitored between pulses to produce the decay spectrum. The lifetime values (τ) were obtained by fitting the decay spectra using OriginLab™ software.

Instrumentation and spectroscopy measurement

NMR spectra were recorded from a Bruker Advance–III 400 NMR spectrometer (at Department of Chemistry and Biomolecular Science, Clarkson University, NY) and a JEOL 400 MHz (at Department of Chemistry, St. Lawrence University, NY), nuclear magnetic resonance (NMR) spectrometer, which are operating at 400 MHz for ^{1}H and 101 MHz for $^{13}C\{^{1}H\}$, respectively. Chemical shifts are quoted in ppm. ^{1}H and ^{13}C chemical shifts were referenced internally with solvent residue chemical shift values ($CDCl_3$: ^{1}H 7.26 ppm, ^{13}C 77.16 ppm; CD_3CN: ^{1}H 1.94 ppm, ^{13}C 1.32 ppm; $(CD_3)_2SO$: ^{1}H 2.50 ppm, ^{13}C 39.52 ppm). NMR data were processed using MestReNova Software. High-resolution mass spectra (HRMS) were recorded using a SCIEX X500B QTOF mass spectrometer (at Center for Air and Aquatic Resources Engineering and Sciences, CAARES, Clarkson university, NY) which operated in positive ion mode (+ve ESI).

Mammalian cell culture

RAW 264.7 cells were purchased from ATCC (Manassas, VA, USA). These cell lines were maintained in Dulbecco's Modified Eagle's Medium (DMEM) supplemented with 10% heat-inactivated fetal bovine serum, Pen-Strep (100 U/mL–100 µg/mL). Pen-Strep was purchased from (Thermo Fisher Scientific, CA, USA). DMEM and fetal bovine serum was purchased from Corning (Corning, NY, USA). Cell lines were cultured in 37 °C with 5% CO_2 atmosphere.

Cell viability assay

$0.1-0.4\times10^{5}$ cells were seeded in 96 well culture plate overnight. Cells were treated with complex **1** for 18 h. The CellTiter-Blue® Cell Viability Assay was then performed according to the manufacturers' protocol (Promega, Madison, Wi, USA). Plates were read using SpectraMax™ i3/i3x multi-mode plate reader.

Declaration of interests

The authors declare no competing financial interests.

Acknowledgements

This work was supported by NIH grants R35GM147112 (K.L.), R35GM147112-02S2 (K.L.), R35GM147112-02S1 (K.L. & M.S.), and Clarkson University start-up fund. We extend our sincere gratitude to St. Lawrence University for generously providing access to their JEOL 400 MHz nuclear magnetic resonance (NMR) spectrometer. The authors acknowledge the use of facilities and instrumentation supported by NSF through the Cornell University Materials Research Science and Engineering Center DMR-1719875.

Author contributions

J.M., F.T, wrote the manuscript. All authors discussed the results and commented on the manuscript. J.M., N.O and F.T wrote the supporting information. Complex **1** was synthesized by J.M., N.O, F.T., M.S. and X.L. The photophysical properties of Complex **1** dyes were investigated by J.M., F.T and M.S. The *in vitro* calibrations were performed by J.M., F.T, and M.S. Fluorescence lifetime measurements were performed by J.M. The selectivity assays were performed by J.M and M.S.

References

1. Kim, M. J., Cheng, G. & Agrawal, D. K. Cl- channels are expressed in human normal monocytes: a functional role in migration, adhesion and volume change. *Clin. Exp. Immunol.* **138**, 453–459 (2004).
2. Diaz, R. J. *et al.* Enhanced cell-volume regulation in cyclosporin A cardioprotection. *Cardiovasc. Res.* **98**, 411–419 (2013).
3. Jentsch, T. J. Chloride and the endosomal-lysosomal pathway: emerging roles of CLC chloride transporters. *J Physiol (Lond)* **578**, 633–640 (2007).
4. Chakraborty, K., Leung, K. & Krishnan, Y. High lumenal chloride in the lysosome is critical for lysosome function. *eLife* **6**, e28862 (2017).
5. Wang, Y. *et al.* CLN7 is an organellar chloride channel regulating lysosomal function. *Sci. Adv.* **7**, eabj9608 (2021).
6. Zhang, Q., Li, Y., Jian, Y., Li, M. & Wang, X. Lysosomal chloride transporter CLH-6 protects lysosome membrane integrity via cathepsin activation. *J. Cell Biol.* **222**, (2023).
7. Zajac, M. *et al.* What biologists want from their chloride reporters - a conversation between chemists and biologists. *J. Cell Sci.* **133**, (2020).
8. Poët, M. *et al.* Lysosomal storage disease upon disruption of the neuronal chloride transport protein ClC-6. *Proc Natl Acad Sci USA* **103**, 13854–13859 (2006).
9. Platt, F. M., d'Azzo, A., Davidson, B. L., Neufeld, E. F. & Tifft, C. J. Lysosomal storage diseases. *Nat. Rev. Dis. Primers* **4**, 27 (2018).
10. Kasper, D. *et al.* Loss of the chloride channel ClC-7 leads to lysosomal storage disease and neurodegeneration. *EMBO J.* **24**, 1079–1091 (2005).
11. Futerman, A. H. & van Meer, G. The cell biology of lysosomal storage disorders. *Nat. Rev. Mol. Cell Biol.* **5**, 554–565 (2004).
12. Schwiebert, E. M., Benos, D. J., Egan, M. E., Stutts, M. J. & Guggino, W. B. CFTR is a conductance regulator as well as a chloride channel. *Physiol. Rev.* **79**, S145-66 (1999).
13. Biwersi, J. & Verkman, A. S. Cell-permeable fluorescent indicator for cytosolic chloride. *Biochemistry* **30**, 7879–7883 (1991).
14. Jayaraman, S., Haggie, P., Wachter, R. M., Remington, S. J. & Verkman, A. S. Mechanism and cellular applications of a green fluorescent protein-based halide sensor. *J. Biol. Chem.* **275**, 6047–6050 (2000).
15. Verkman, A. S., Takla, R., Sefton, B., Basbaum, C. & Widdicombe, J. H. Quantitative fluorescence measurement of chloride transport mechanisms in phospholipid vesicles. *Biochemistry* **28**, 4240–4244 (1989).
16. Prakash, V., Saha, S., Chakraborty, K. & Krishnan, Y. Rational design of a quantitative, pH-insensitive, nucleic acid based fluorescent chloride reporter. *Chem. Sci.* **7**, 1946–1953 (2016).
17. Koncz, C. & Daugirdas, J. T. Use of MQAE for measurement of intracellular [Cl-] in cultured aortic smooth muscle cells. *Am. J. Physiol.* **267**, H2114-23 (1994).
18. Park, S.-H., Shin, I., Kim, Y.-H. & Shin, I. Mitochondrial Cl--Selective Fluorescent Probe for Biological Applications. *Anal. Chem.* **92**, 12116–12119 (2020).
19. Park, S.-H., Hyun, J. Y. & Shin, I. A lysosomal chloride ion-selective fluorescent probe for biological applications. *Chem. Sci.* **10**, 56–66 (2019).
20. Sonawane, N. D., Thiagarajah, J. R. & Verkman, A. S. Chloride concentration in endosomes measured using a ratioable fluorescent Cl- indicator: evidence for chloride accumulation during acidification. *J. Biol. Chem.* **277**, 5506–5513 (2002).
21. Baggaley, E. *et al.* Long-lived metal complexes open up microsecond lifetime imaging microscopy under multiphoton excitation: from FLIM to PLIM and beyond. *Chem. Sci.* **5**, 879–886 (2014).
22. Dmitriev, R. I., Intes, X. & Barroso, M. M. Luminescence lifetime imaging of three-dimensional biological objects. *J. Cell Sci.* **134**, 1–17 (2021).
23. Wu, C. *et al.* Design strategies of iridium(III) complexes for highly efficient saturated blue phosphorescent OLEDs with improved lifetime. *EnergyChem* **6**, 100120 (2024).
24. Tritton, D. N. *et al.* Development and advancement of iridium(III)-based complexes for photocatalytic hydrogen evolution. *Coord. Chem. Rev* **459**, 214390 (2022).

25. Lee, L. C.-C. & Lo, K. K.-W. Shining new light on biological systems: luminescent transition metal complexes for bioimaging and biosensing applications. *Chem. Rev.* **124**, 8825–9014 (2024).
26. Ho, P.-Y., Ho, C.-L. & Wong, W.-Y. Recent advances of iridium(III) metallophosphors for health-related applications. *Coord. Chem. Rev* **413**, 213267 (2020).
27. Rupp, M. T., Shevchenko, N., Hanan, G. S. & Kurth, D. G. Enhancing the photophysical properties of Ru(II) complexes by specific design of tridentate ligands. *Coord. Chem. Rev* **446**, 214127 (2021).
28. Goodall, W. & Williams, J. A. G. Iridium(III) bis-terpyridine complexes incorporating pendent N-methylpyridinium groups: luminescent sensors for chloride ions†. *J. Chem. Soc., Dalton Trans.* 2893–2895 (2000) doi:10.1039/b005046f.
29. Buchberger, W. Determination of iodide and bromide by ion chromatography with post-column reaction detection. | Semantic Scholar. *Journal of Chromatography A* (1988).
30. Olszowy, H. A., Rossiter, J., Hegarty, J. & Geoghegan, P. Background levels of bromide in human blood. *J. Anal. Toxicol.* **22**, 225–230 (1998).

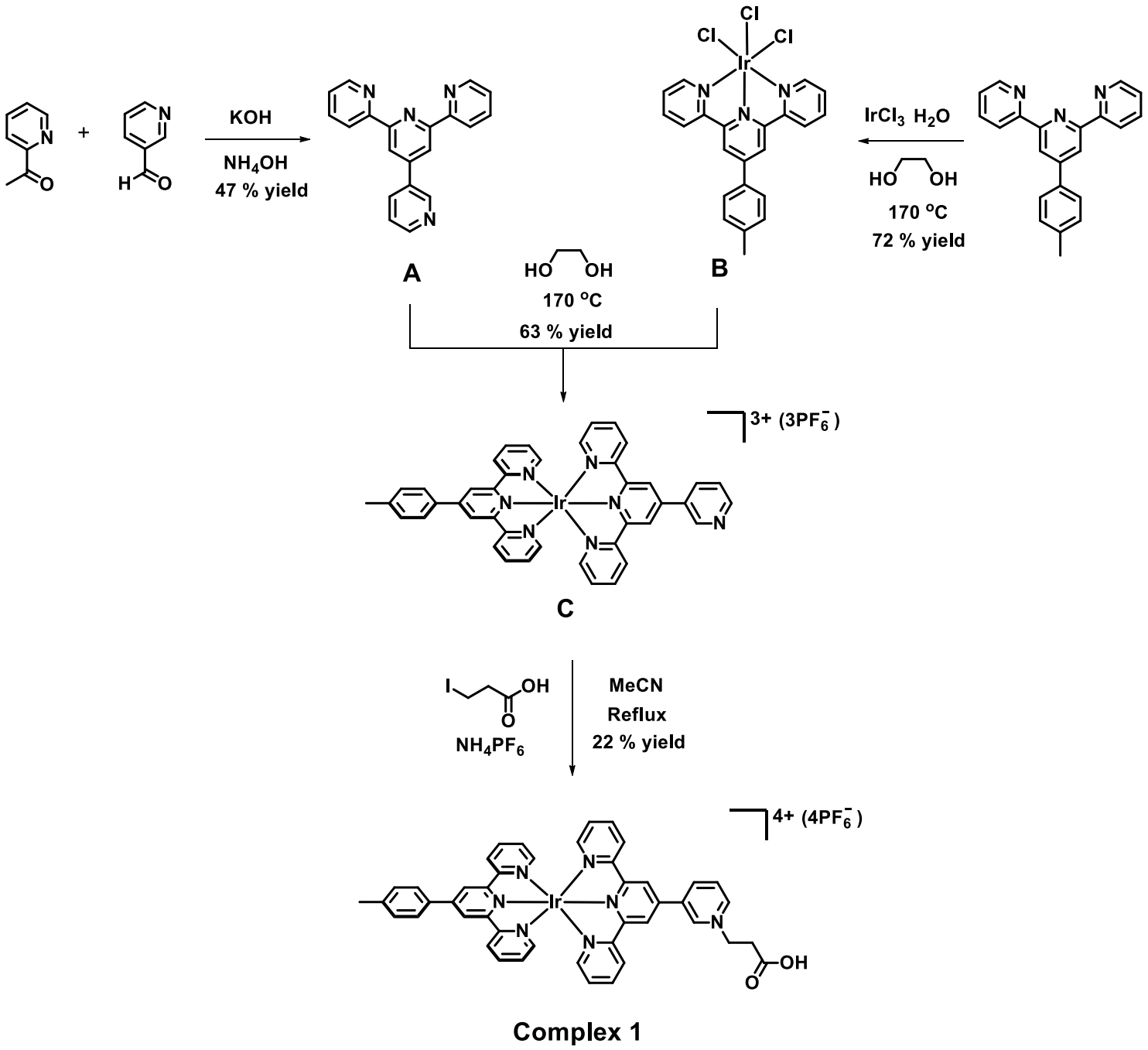

Figure 1. Synthetic route Complex **1**.

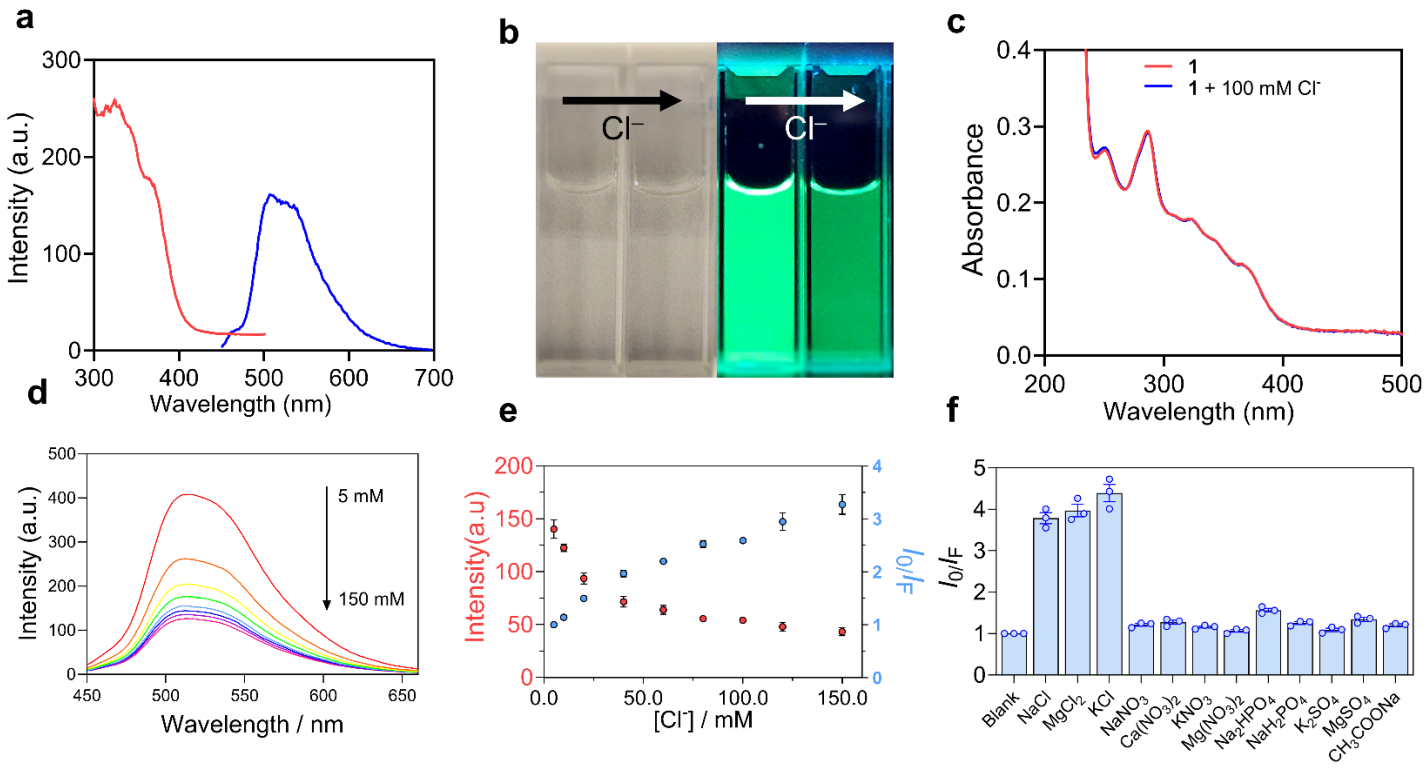

Figure 2. Complex 1 detects chloride selectively and sensitively.

(**a**) Excitation and emission spectrum of complex **1**. (**b**) Cuvette photos showing emission of **1** with and without 100 mM Cl^-. (**c**) Absorption spectrum of complex **1** with and without 100 mM Cl^-. (**d**) Emission spectrum of **1** in the presence of 5−150 mM Cl^- under excitation wavelength at 360 nm. (**e**) Luminescence Intensity at 510 nm (red) and Stern-Volmer plot (blue) of **1** (10 μM) with increasing [Cl^-] in sodium phosphate buffer (20 mM, pH 7.2) upon excitation at 360 nm. Normalized emission intensity ratio (I_0/I_F) of **1** was represented as a function of Cl^- concentration. Values were normalized to I_0/I_F at [Cl^-] = 5 mM. (**f**) Luminescence response of **1** given by the fold change in I_0/I_F in the presence of different ionic salts (150 mM). Error bars indicate the mean ± standard error of the mean (s.e.m.) of three independent measurements.

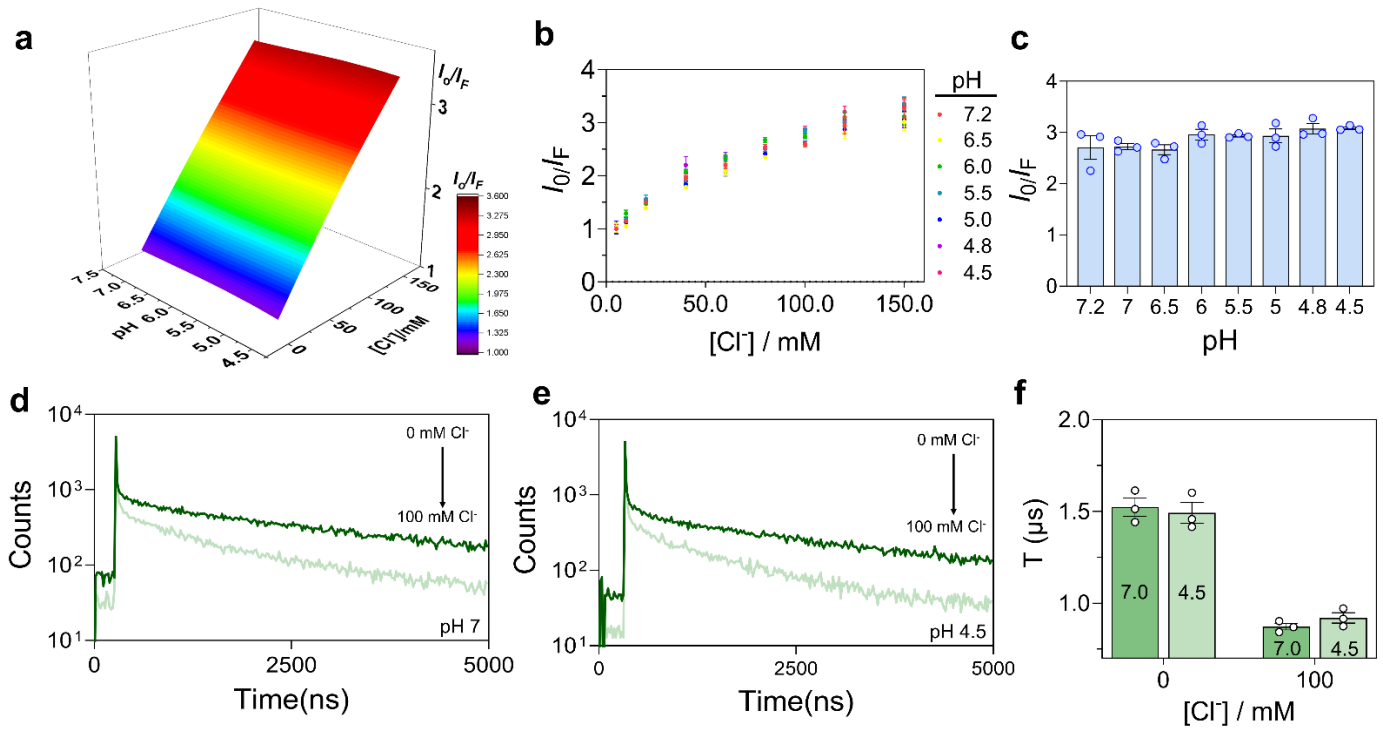

Figure 3. Complex 1 detects chloride in a pH independent manner.

(**a**) Calibration surface plot of I_0/I_F of **1** as a function of Cl^- and pH. (**b**) Stern-Volmer plot of **1** (10 μM) with increasing [Cl^-] in sodium phosphate buffer (20 mM) upon excitation at 360 nm. Normalized emission intensity ratio (I_0/I_F) of **1** was represented as a function of Cl^- concentration at pH 4.5, 4.8, 5.0, 5.5, 6.0, 6.5, and 7.2. Values were normalized to I_0/I_F at [Cl^-] at 5 mM. (**c**) Luminescence response of **1** at different pH values and fold changes in I_0/I_F were shown. (**d-e**) Phosphorescence lifetime measurement of complex **1** with 0 mM or 100 mM Cl^- in sodium phosphate buffers (20 mM, pH 7 or pH 4.5). (**f**) Comparison of phosphorescence lifetime values derived from the lifetime decay plots (**d/e**). Error bars indicate the mean ± standard error of the mean (s.e.m.) of three independent measurements.

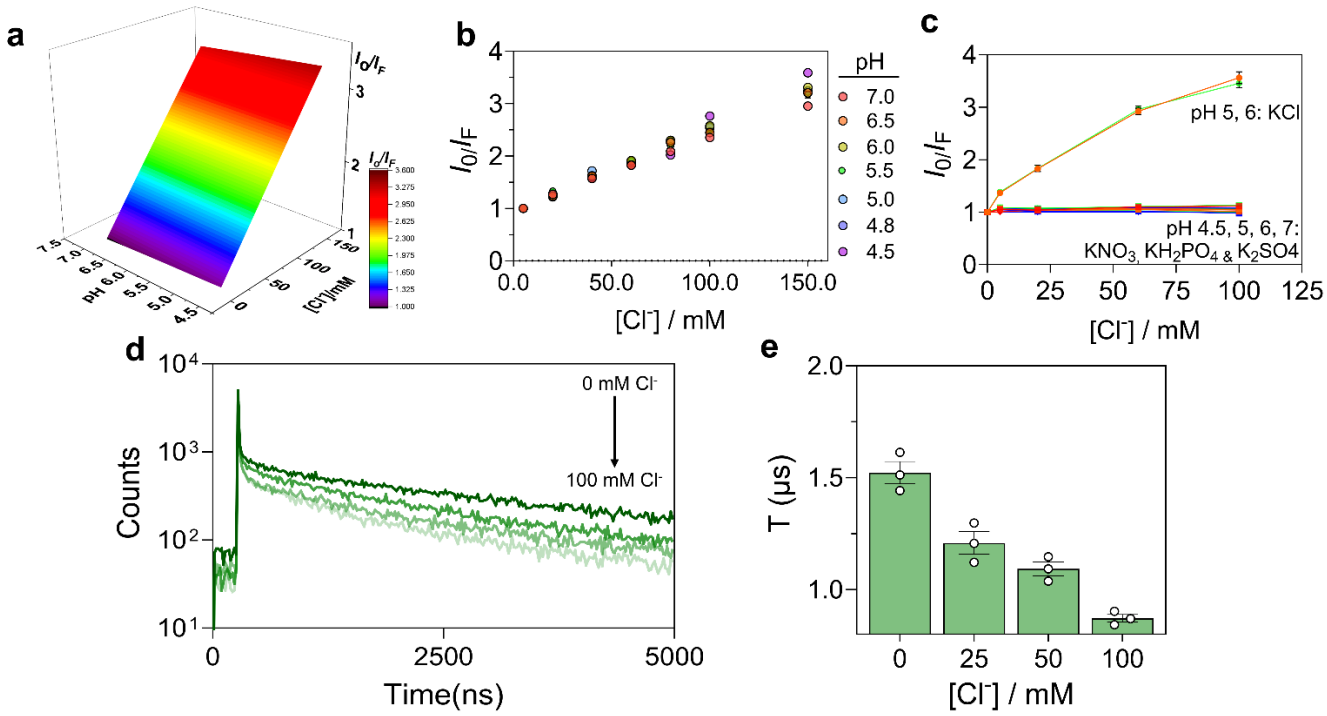

Figure 4. Complex 1 selectively detects chloride in physiological ionic environment.

(**a**) Calibration surface plot of I_0/I_F of **1** as a function of Cl^- and pH measured in 20 mM sodium phosphate buffer with physiological3 ionic environment (150 mM KNO_3, 5 mM $NaNO_3$, 1 mM $Ca(NO_3)_2$ and 1 mM $Mg(NO_3)_2$). (**b**) Stern-Volmer plot of **1** (10 µM) with increasing [Cl^-] different pH values upon excitation at 360 nm. Normalized emission intensity ratio (I_0/I_F) of **1** represented as a function of Cl^- concentration at pH 4.5, 4.8, 5.0, 5.5, 6.0, 6.5, and 7.0. Values were normalized to I_0/I_F at [Cl^-] at 5 mM. (**c**) Luminescence response of **1** at different pH values given by the fold change in I_0/I_F from 0 mM to 100 mM of each indicated ions. (**d**) Phosphorescence lifetime spectrum of complex **1** upon addition of 0−100 mM Cl^- in sodium phosphate buffer (5 mM, pH 7) with physiological ionic environment (150 mM KNO_3, 5 mM $NaNO_3$, 1 mM $Ca(NO_3)_2$ and 1 mM $Mg(NO_3)_2$). (**e**) Phosphorescence lifetime values derived from lifetime decay plot (**d**) in varying chloride environments ([Cl^-] = 0, 25, 50 and 100 mM). Error bars indicate the mean ± standard error of the mean (s.e.m.) of three independent measurements.

Leveraging Metal Complexes for Microsecond Lifetime-Based Chloride Sensing

Jared Morse[†1], Nnamdi Ofodum[†1], Fung-Kit Tang[†1], Matthias Schmidt[1], Xiaocun Lu[1*], Kaho Leung[1*]

[1]*Department of Chemistry & Biomolecular Science, Clarkson University, NY, 13676, United States*

**Correspondence to: xlu@clarkson.edu (X.L.), kleung@clarkson.edu (K.L.)*

[†]*These authors contributed equally.*

Synthesis

Synthesis of compound **A**. Compound **A** was synthesized using a modified procedure from the literature.[1] In brief, 2-acetylpyiridine (2.42 g, 19.9 mmol) and 3-pyridinecarboxaldehyde (1.1 g, 10.3 mmol) were dissolved in EtOH (1 mL) and 30% ammonia solution (30 mL). Then KOH (1.6 g, 28.5 mmol) was added, the mixture was stirred at room temperature for 4 h. The gelatinous solid was filtered, washed with cold water and the product was purified by recrystallization using EtOH to yield a white solid. Yield: 1.5 g, 47%. ^{1}H NMR (400 MHz, $CDCl_3$, 298K) δ 9.13 (d, *J* = 2.4 Hz, 1H), 8.81 – 8.65 (m, 7H), 8.18 (dt, *J* = 7.9, 1.9 Hz, 1H), 7.89 (td, *J* = 7.8, 1.7 Hz, 2H), 7.45 (dd, *J* = 7.9, 4.8 Hz, 1H), 7.39 – 7.31 (m, 2H). HRMS (+ve ESI): calculated for $C_{20}H_{15}N_4^+$ $[M+H]^+$ *m/z* 311.1291, found 311.1313.

Synthesis of compound **B**. Compound **B** was synthesized using a modified procedure from the literature.[2] 4-(*p*-Tolyl)-2,2:6,2-terpyridine (304 mg, 0.94 mmol) iridium chloride monohydrate (328 mg, 1.04 mmol) were dissolved in ethylene glycol (15 mL) and heated at 170 ℃ for 12 min. The reaction was allowed to cool to room temperature and the dark red precipitate was isolated by filtration. The precipitate solid was washed water, then EtOH followed by diethyl ether, the precipitate was finally dried in air. Yield: 416 mg, 72%. ^{1}H NMR (400 MHz, $(CD_3)_2SO$, 298K) δ 9.22 (d, *J* = 5.4 Hz, 2H), 9.08 (s, 2H), 8.91 (d, *J* = 8.0 Hz, 2H), 8.29 (td, *J* = 7.9, 1.4 Hz, 2H), 8.14 (d, *J* = 8.2 Hz, 2H), 8.01 – 7.90 (m, 2H), 7.51 (d, *J* = 8.0 Hz, 2H), 2.48 (s, 3H). HRMS (+ve ESI): calculated for $C_{22}H_{17}Cl_2IrN_3^+$ $[M\text{-}Cl]^+$ *m/z* 586.0423, found 586.0458.

Synthesis of compound **C**. Compound **C** was synthesized using a modified procedure from the literature.[2] Compound **A** (108 mg, 0.348 mmol) and compound **B** (196 mg, 0.315 mmol) were dissolved in ethylene glycol (15 mL), then the mixture was heated at 170 ℃ for 24 h. The mixture was diluted with water (200 mL) and excess NH_4PF_6 was added. The brown precipitate was collected by filtration, washed with water and dried in air to yield brown solid. Yield: 252 mg, 63%. ^{1}H NMR (400 MHz, CD_3CN, 298K) δ 9.38 (d, *J* = 1.8 Hz, 1H), 9.09 (d, *J* = 19.0 Hz, 4H), 8.92 (d, *J* = 4.8 Hz, 1H), 8.76 – 8.67 (m, 4H), 8.56 – 8.52 (m, 1H), 8.29 – 8.19 (m, 4H), 8.13 (d, *J* = 8.1 Hz, 2H), 7.79 (dd, *J* = 8.0, 4.9 Hz, 1H), 7.70 (t, *J* = 6.1 Hz, 4H), 7.64 (d, *J* = 8.0 Hz, 2H), 7.55 – 7.46 (m, 4H), 2.58 (s, 3H). ^{13}C NMR (101 MHz, CD_3CN, 298K) δ 159.09, 158.89, 157.11, 155.86, 155.48, 154.41, 154.38, 154.34, 153.51, 150.11, 144.13, 143.88, 143.80, 136.83, 133.36, 132.37, 131.54, 130.89, 130.74, 129.36, 128.46, 128.35, 125.58, 125.42, 124.91, 21.55. HRMS (+ve ESI): calculated for $C_{42}H_{31}IrN_7PF_6^{2+}$ $[M]^{2+}$*m/z* 485.5951, found 485.5940.

Synthesis of complex **1**. 3-Iodopropionic acid (1.1 g, 5.5 mmol) was added to a solution of compound **C** (171 mg, 0.136 mmol) in MeCN (25 mL). Then NH_4PF_6 (75 mg, 0.46 mmol) was added, and the mixture was refluxed for 72 h. Solvent was removed and the residue was purified by column chromatography using MeCN/saturated aqueous KNO_3 (*v/v* = 2:1). The collected product was redissolved in acetonitrile and saturated NH_4PF_6 solution was added to form the precipitates. The precipitate was collected via filtration to give yellow powder as product. Yield: 45 mg, 22 %. ^{1}H NMR (400 MHz, CD_3CN, 298K) δ 9.60 (s, 1H), 9.36 – 9.21 (m, 3H), 9.17 – 9.09 (m, 3H), 8.77 (d, *J* = 8.0 Hz, 4H), 8.47 (t, *J* = 6.5 Hz, 1H), 8.37 – 8.23 (m, 4H), 8.17 (d, *J* = 6.6 Hz, 2H), 7.83 (d, *J* = 5.1 Hz, 4H), 7.72 – 7.53 (m, 6H), 5.06 (t, *J* = 5.9 Hz, 2H), 3.34 (t, *J* = 5.3 Hz, 2H), 2.58 (s, 3H).^{13}C NMR (101 MHz, CD_3CN, 298 K) δ 171.06, 158.04, 158.00, 157.67, 157.36, 156.14, 156.07, 155.43, 155.06, 154.40, 154.36, 153.61, 153.46, 153.32, 148.53, 143.02, 142.78, 136.26, 132.41, 130.46, 129.83, 128.40, 127.50, 127.24, 125.13, 123.87, 58.07, 33.66, 20.55. HRMS (+ve ESI): calculated for $C_{45}H_{36}IrN_7O_2P_2F_{12}^{2+}$ $[M]^{2+}$ *m/z* 594.5916, found 594.5943.

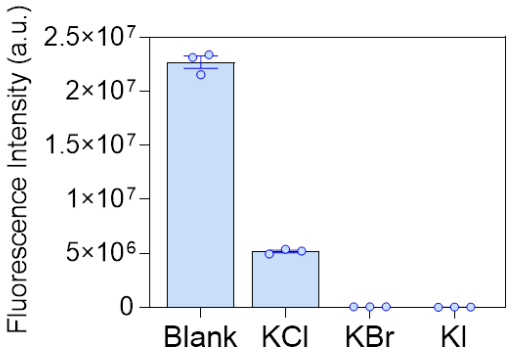

Figure S1. Complex **1** is halide sensitive. Fluorescence intensity of complex **1** in the presence of 100 mM of chloride, bromide, or iodide. Error bars indicate the mean ± standard error of the mean (s.e.m.) of three independent measurements.

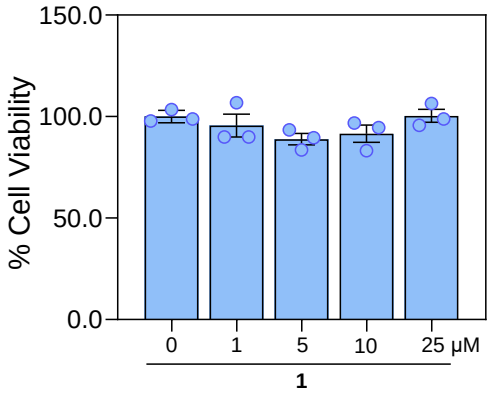

Figure S2. Cell toxicity analysis of Complex **1** in RAW 264.7 murine macrophages. Error bars indicate the mean ± standard error of the mean (s.e.m.) of three independent measurements.

Characterization of compound A

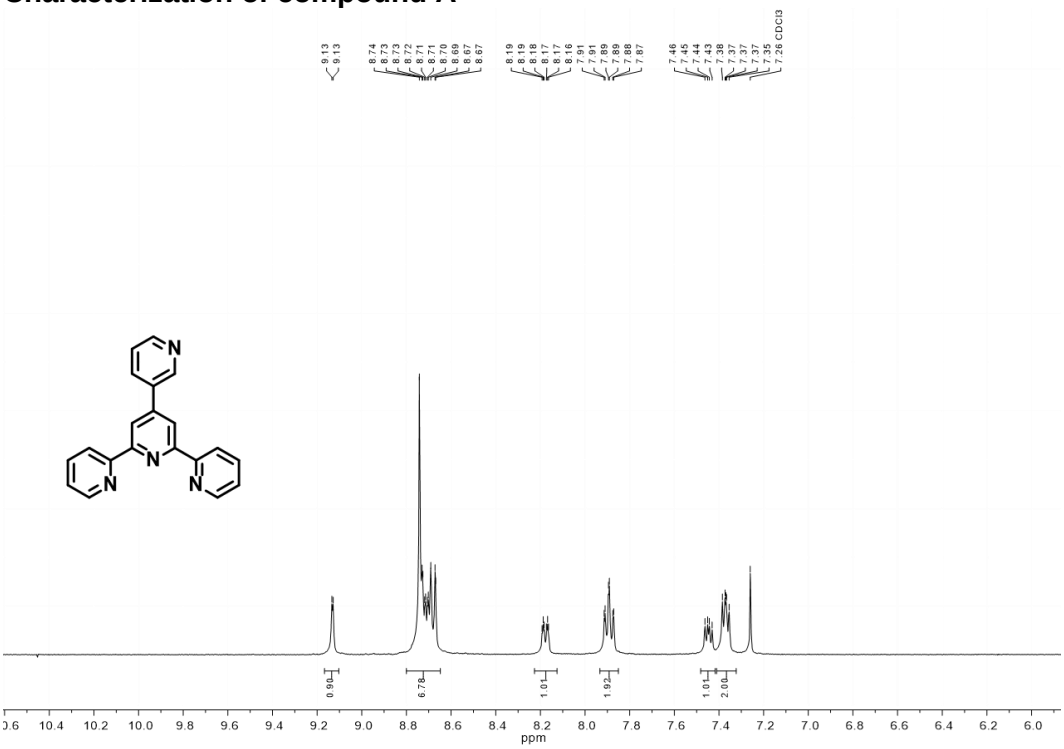

Figure S3. ^{1}H NMR spectrum (400 MHz, $CDCl_3$, 298K) of compound **A**.

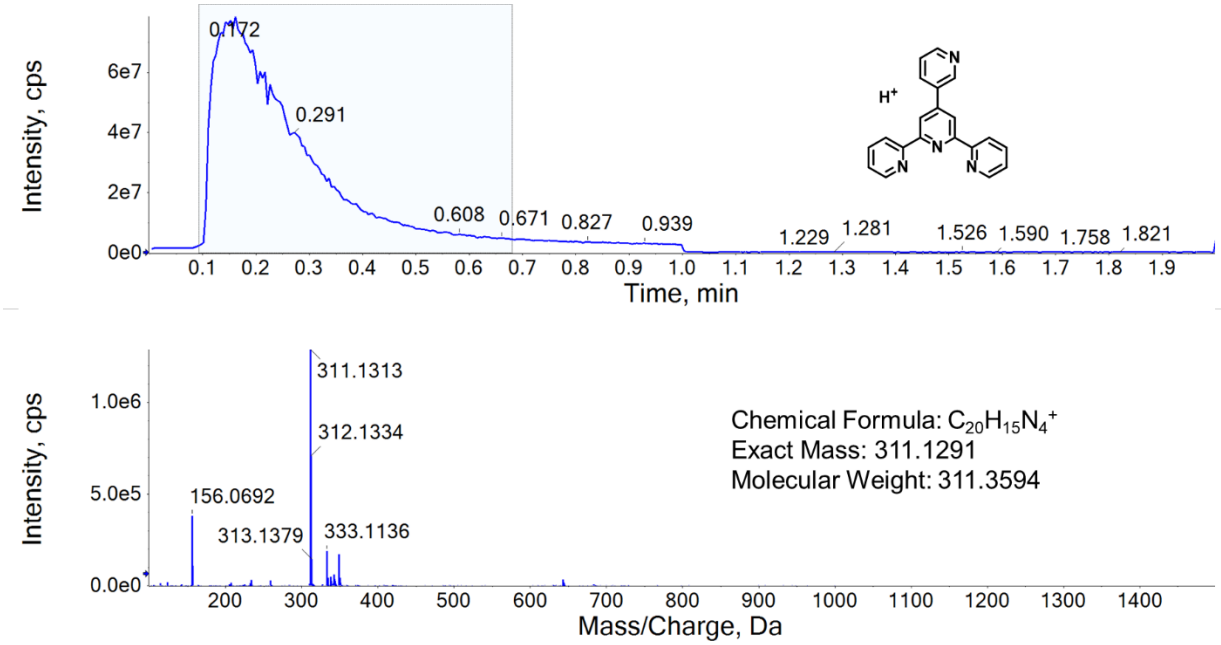

Figure S4. HRMS (+ve ESI) spectrum of compound **A**.

Characterization of compound B

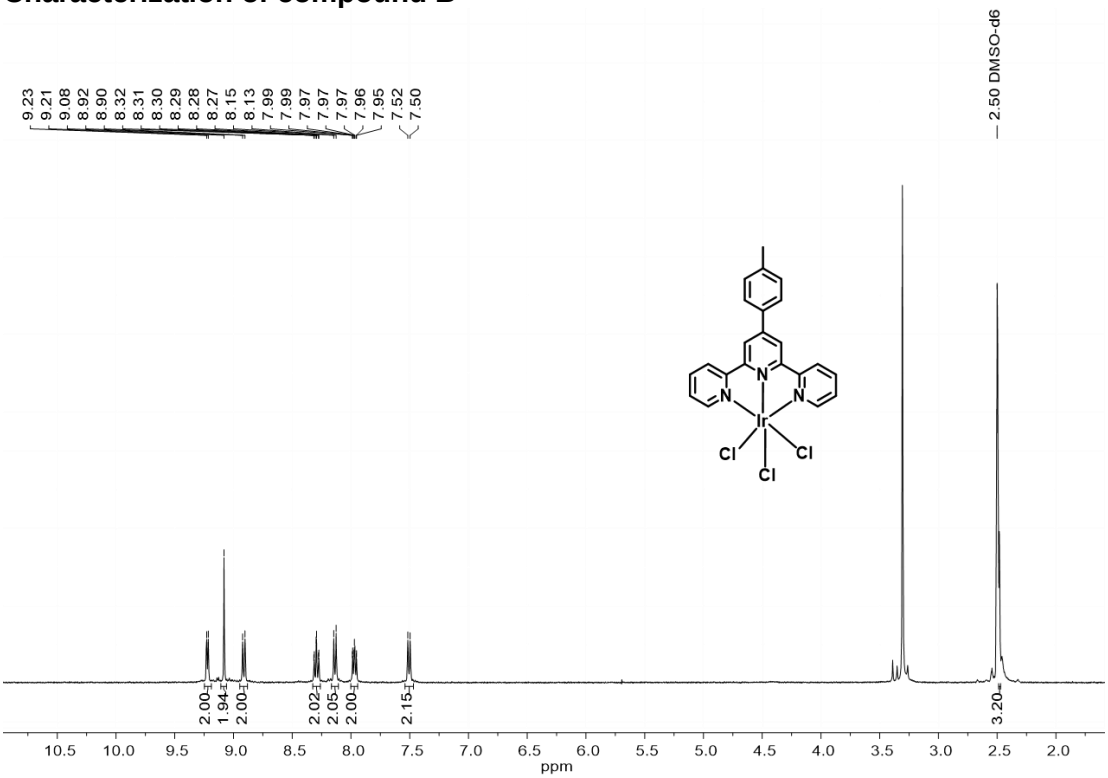

Figure S5. ^{1}H NMR spectrum (400 MHz, $(CD_3)_2SO$, 298K) of compound **B**.

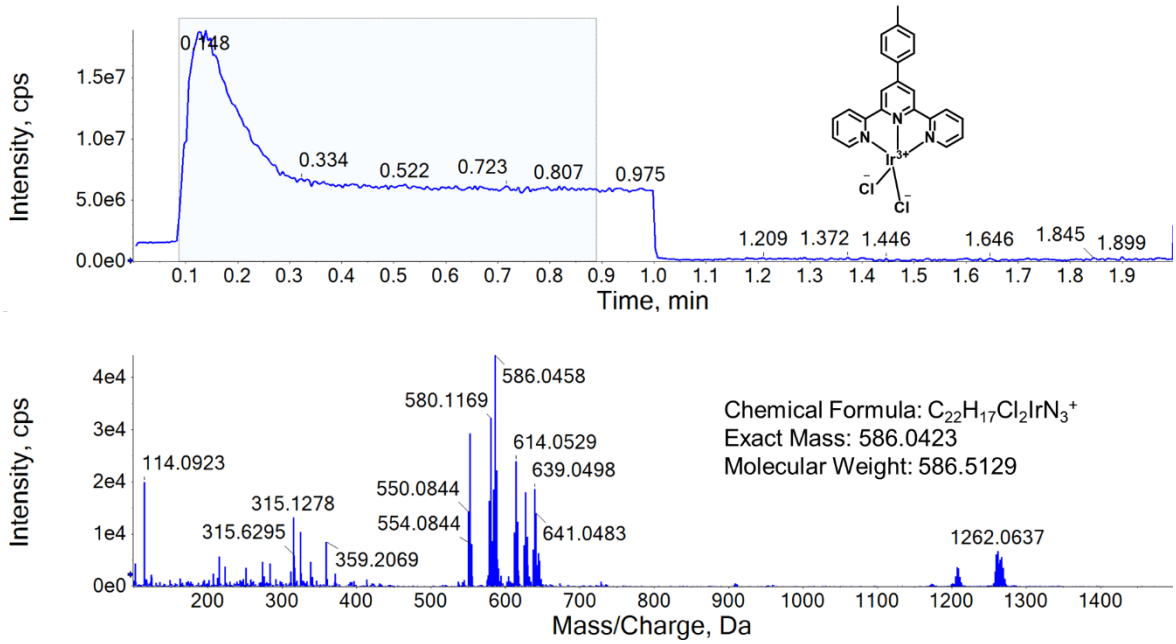

Figure S6. HRMS (+ve ESI) spectrum of compound **B**.

Characterization of compound C

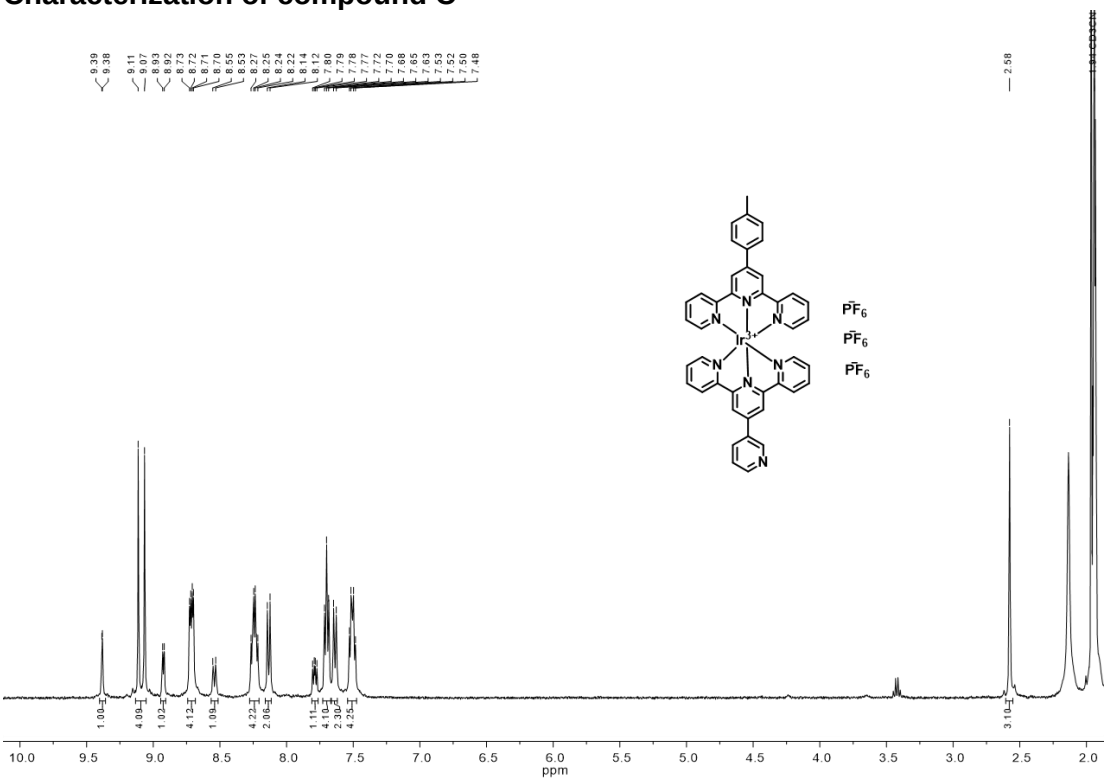

Figure S7. ^{1}H NMR spectrum (400 MHz, CD_3CN, 298K) of compound **C**.

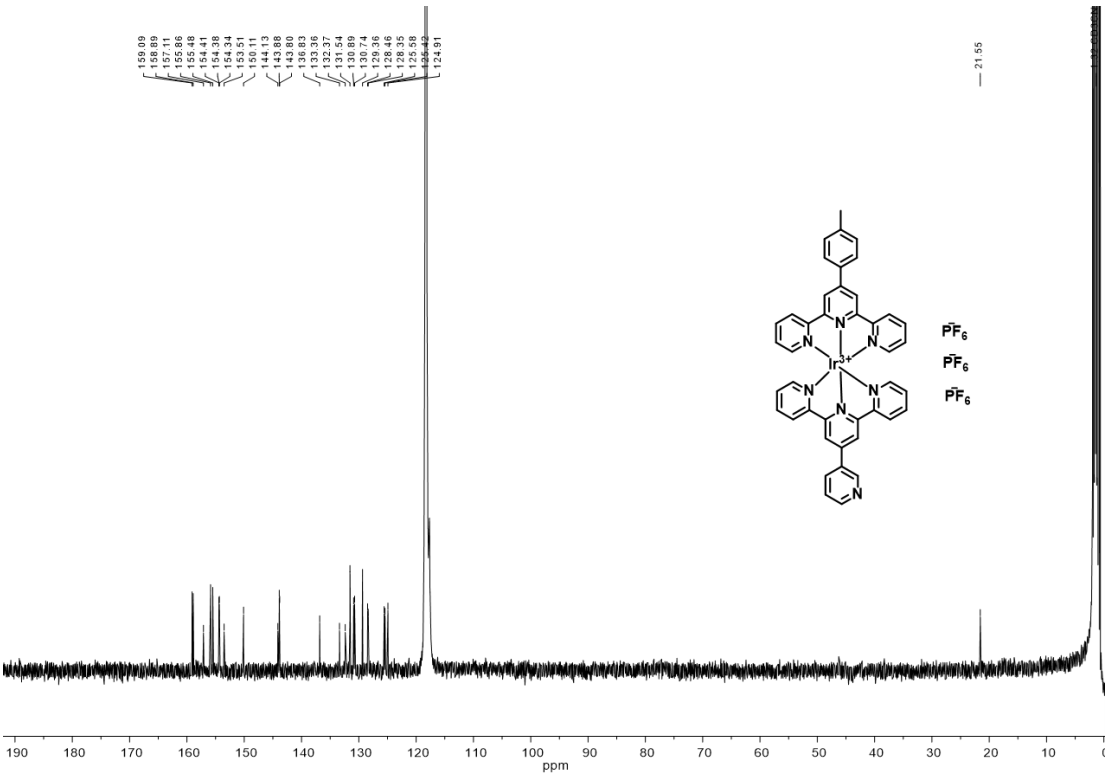

Figure S8. ^{13}C NMR spectrum (101 MHz, CD_3CN, 298 K) of compound **C**.

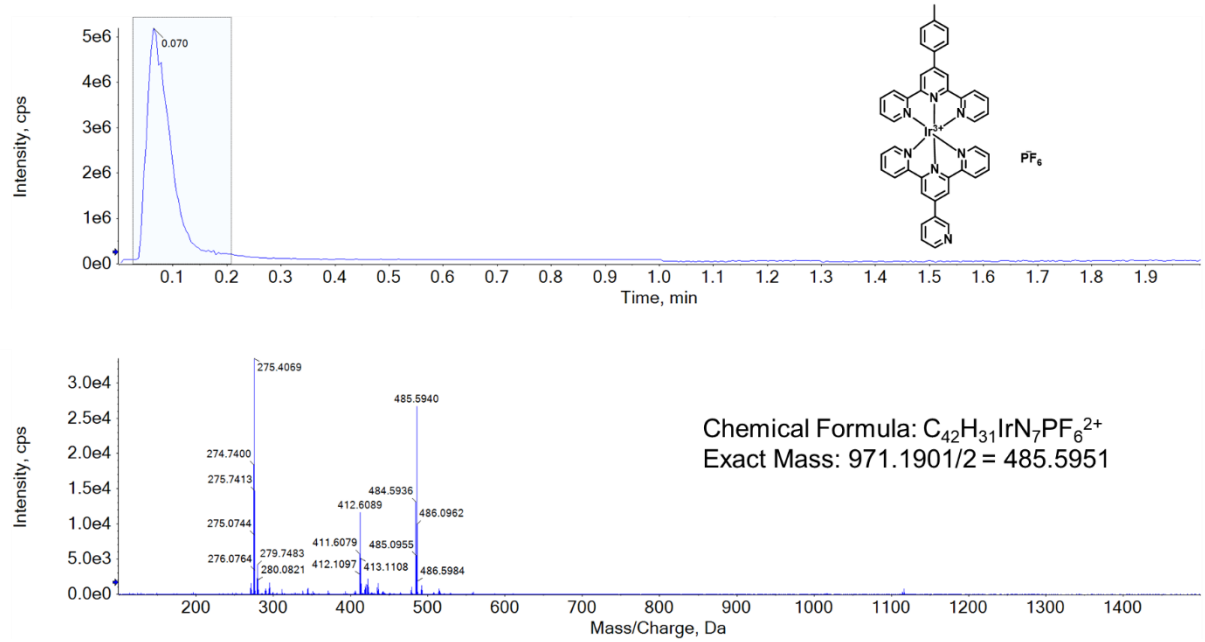

Figure S9. HRMS (+ve ESI) spectrum of compound **C**.

Characterization of complex 1

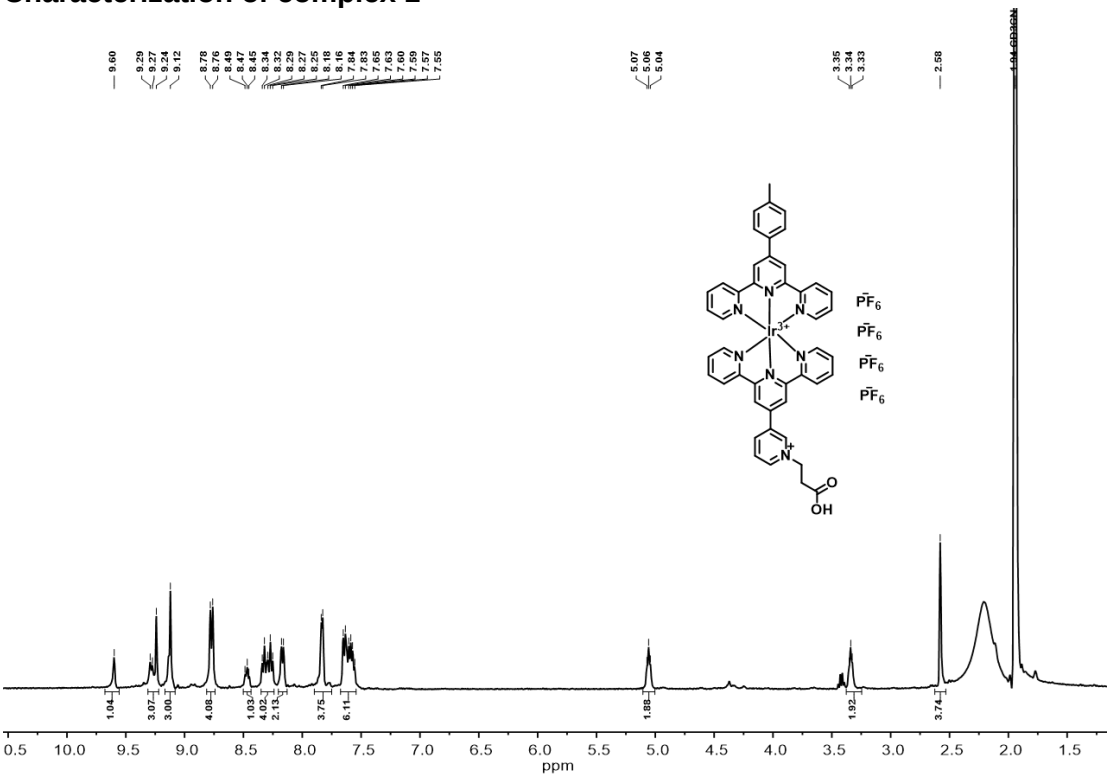

Figure S10. ^{1}H NMR spectrum (400 MHz, CD_3CN, 298K) of complex **1**.

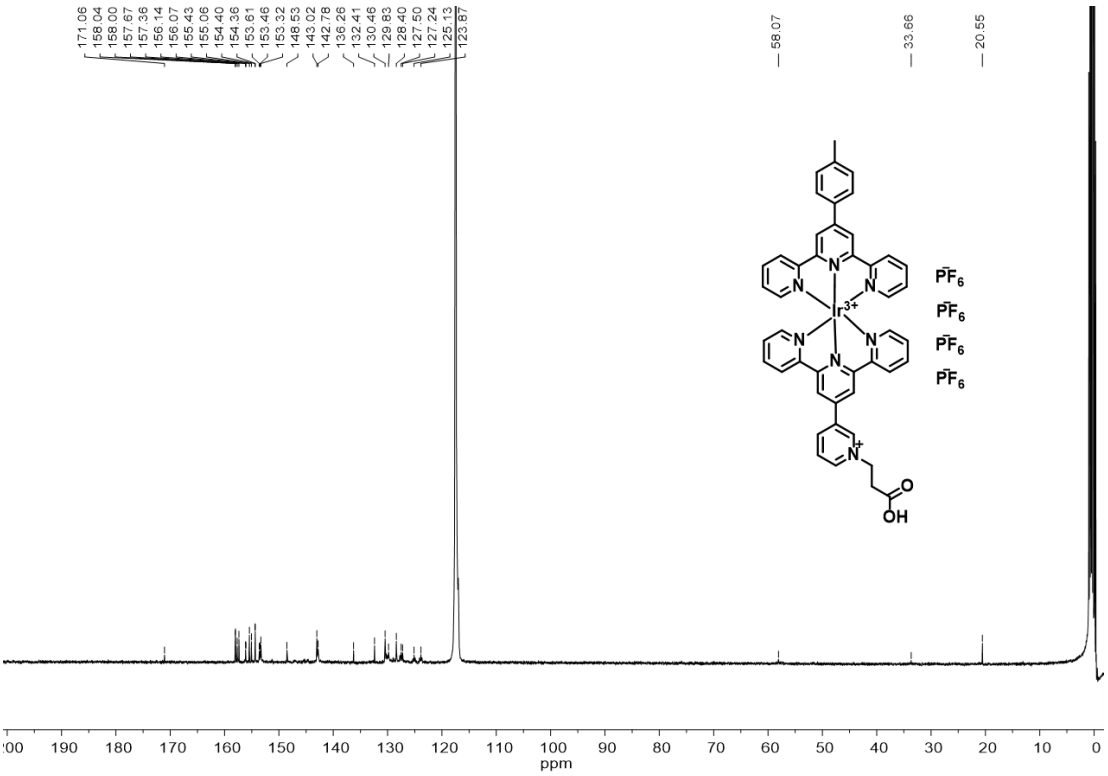

Figure S11. ^{13}C NMR spectrum (101 MHz, CD_3CN, 298 K) of complex **1**.

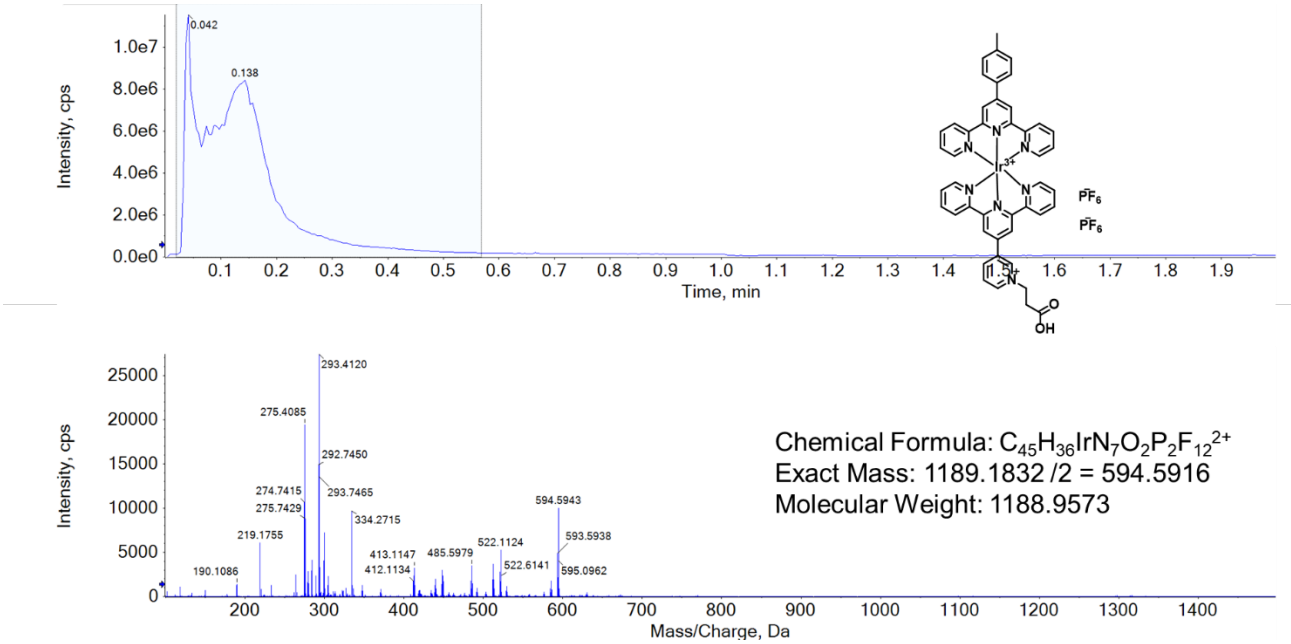

Figure S12. HRMS (+ve ESI) spectrum of complex **1.**

References:

1. Khavasi, H. R.; Esmaeili, M. Case Study of the Correlation between Metallogelation Ability and Crystal Packing. *Cryst. Growth Des.* **2019**, *19* (8), 4369-4377. DOI: 10.1021/acs.cgd.9b00117.

2. Goodall, W.; Williams, J. A. G. Iridium(III) bis-terpyridine complexes incorporating pendent N-methylpyridinium groups: luminescent sensors for chloride ions*J. Chem. Soc., Dalton Trans.* **2000**, (17), 2893-2895, 10.1039/B005046F. DOI: 10.1039/B005046F.